Supplementary Information

High-Performance solar-blind flexible Deep-UV photodetectors based on quantum dots synthesized by femtosecond-laser ablation

*Somak Mitra, Assa Aravindh, Gobind Das, Yusin Pak, Idris Ajia, Kalaivanan Loganathan, Enzo Di Fabrizio, Iman S. Roqan**

King Abdullah University of Science and Technology (KAUST), Thuwal, Saudi Arabia

S1. Fourier transform infrared spectroscopy (FTIR) of C-doped ZnO QDs

In order to verify the surface termination, FTIR analysis was carried out on as-prepared samples and the findings were compared to those pertaining to an aged sample, as shown in Figure S1. FTIR spectra indicate that surface termination likely exists in the sample. FTIR spectra were obtained by employing attenuated total reflectance mode (ATR) in the 500−4000 cm^{-1} wavelength range. [1-3] We observed emergence of a broad band peak at 3200−3500 cm^{-1}, which is attributed to the presence of the hydroxyl on the material surface. Specifically, H-OH stretching contributes to the peak at 3435 cm^{-1}, while those noted at 3446 cm^{-1} and 3500 cm^{-1} correspond to the O-H stretching mode. This broad peak is enhanced in the spectrum pertaining to the aged sample, which was synthesized in ethanol, due to which –OH terminations gradually emerge at the particle surface over time. The symmetric and asymmetric C-H stretching nodes of $–CH_2$ group shown in Fig. S1 overlap with the broad signal pertaining to O-H group. The peaks located between 2800 cm^{-1} and 3000 cm^{-1} correspond to C-H stretching vibration of the alkane group. [1-3] A very pronounced peak at 1586 cm^{-1} is attributed to symmetric stretching of C=O (-R), indicating that a Zn-carboxylate termination is available on the surface of the nanocrystals. [1-3] The shape of the 1586 cm^{-1} peak changes due to ageing, which suggests that QD surfaces are gradually Zn-R terminated, where R represents COO-, C=O, etc. Asymmetrical stretching of Zn carboxylate is also observed at ~1630 cm^{-1}. [1-3] The peaks located around 1454 cm^{-1} and 1384 cm^{-1} correspond to stretching and wagging of CH_2. [1-3] This result confirms the contribution of carbon-related components and hydroxyl group on the surface of QDs. At the same time, FTIR spectrum suggests that QD surface-termination is of the –R type, which prevents further oxidation of the core level of the QDs.

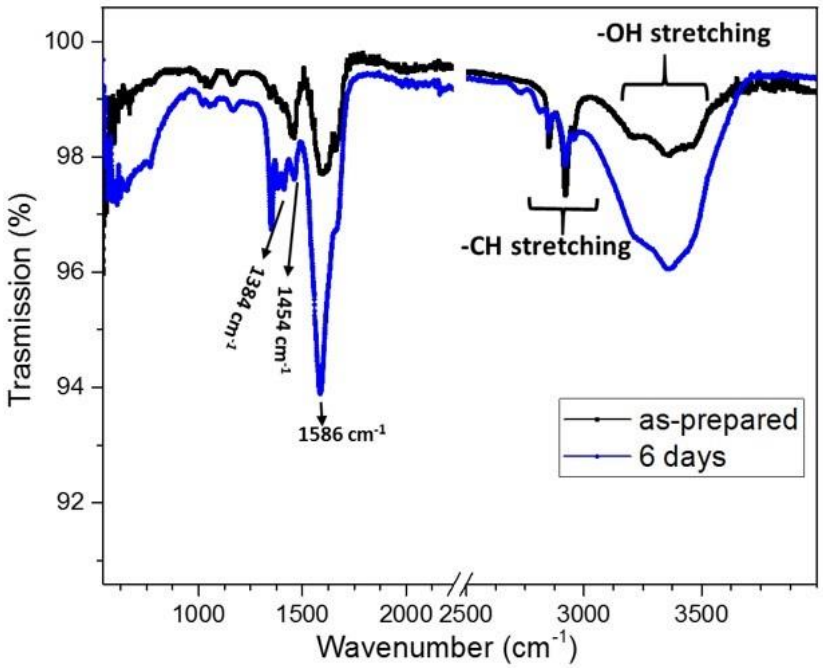

Figure S1. Fourier transform infrared transmission signal of as-prepared ZnO QDs and QDs aged in ethanol.

S2. Raman Spectrum of C-doped ZnO Quantum Dots

Figure S2 depicts the Raman spectra of C-doped ZnO quantum dots (QDs). All Raman measurements were performed using WiTec Raman system, equipped with 532 nm laser source, 100× objective, and 600 lines/mm grating. ZnO QDs were drop-casted and dried on calcium fluoride (CaF_2) substrate. Various Raman measurements were performed at different locations. The Raman spectra show a clear contribution of ZnO QDs, C-H vibration, and C-cluster. The sharp peak at around 317 cm^{-1} is related to the Ca-F vibration of the substrate over which the ZnO QDs sample was drop-casted. The peak at 438 cm^{-1} is attributed to the ZnO wurtzite structure, specifically to the E_2 (high) vibration mode of ZnO, as shown in Figure S2 a. [4-7] The second peak observed at 566 cm^{-1} is attributed to the E_1 (LO) ZnO nanostructure mode. [4-7] The peak

corresponding to pure ZnO is attributed to the intrinsic defect states. [4-7] The peak located in the lowering wavenumber is probably attributed to the Zn-C bonds. [6]

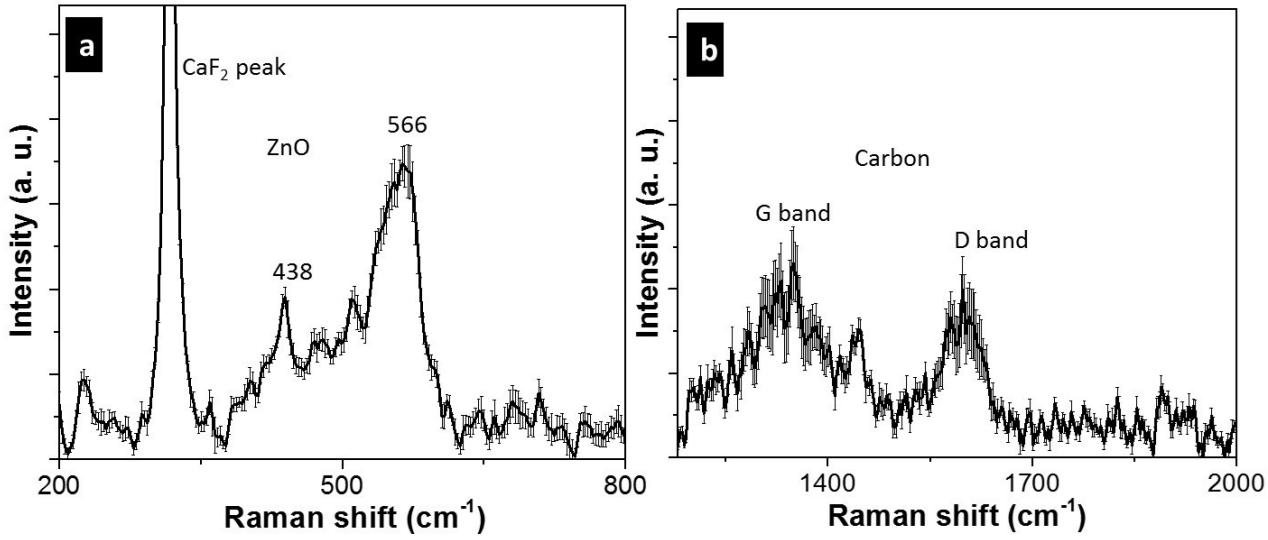

Figure S2. Raman spectrum of C-doped ZnO QDs. (a) Raman spectra originating from ZnO QDs and (b) spectra showing presence of G and D band of carbon.

The existence of C-related Raman-active modes of graphitic (G) and defect (D) bands was observed at 1350 cm^{-1} and 1600 cm^{-1}, respectively, as shown in Figure S2 b. The presence of Raman-active C-related modes confirms the existence of C-ZnO composite. [5] This observation is also verified by the Fourier transform infrared spectroscopy (FTIR), discussed in the following section.

S3. Particle size calculation from absorption measurements

We also estimated the size of QDs based on absorption measurements. The direct bandgap of the ZnO bulk at pH 7.5 is 3.63 eV (E_{bulk}). By examining the absorption spectra of the sample, average particle size can be estimated using the hyperbolic band model, as noted in Equation (1):

$$d = 2\sqrt{\frac{2\pi^2 h^2 E_{bulk}}{m^*({E_N}^2 - {E_{bulk}}^2)}} \qquad (1)$$

where d is the nanoparticle diameter, m^* is the effective mass of the sample ($m^* = 29.15\times10^{-31}$ kg for ZnO), h is Planck's constant (6.626×10^{-34} J s) and E_N denotes particle bandgap, which is estimated at 5 eV from the Tauc plot. [8] Equation (1) yielded an average particle size of 4.6 nm, which is close to the average particle size measured from the TEM images.

S4. Photodetector performance of Device 1 at high bias (>5V)

Figure S3 shows photo-response under pulsed DUV illumination at different bias voltages under illumination of 224 nm (5.5 eV) pulsed laser with energy, which is well above the 4.9 eV bandgap of the QDs. Photodetector responses obtained under different bias voltages revealed that, at lower bias, the response is much more stable, as shown in Figure 5c. Under pulsed laser illumination, at 1 V, 2 V and 5 V bias, a very stable response over time is obtained. This stability does not persist at higher bias voltages (> 5 V), as the transient photocurrent changes at different times, as shown in Figure S3. At 2 V and 5 V, fast response (in ms) is observed, with higher responsivity (up to ~100 mA/W) compared to that measured at 1 V.

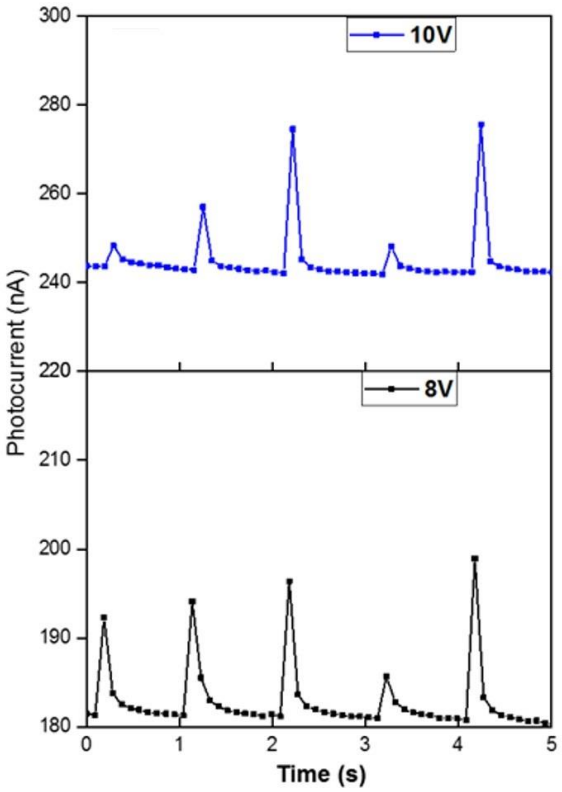

Figure S3. Transient photo-response of Device 1.

Figure S4 shows the fitting of the decay time at different bias voltages for Device 1. The fitting procedure adopted to measure the decay time is in line with that used by other authors. [9-13] The decay curve has been fitted by exponential function $I_{ph} = A_1*\exp(-t/\tau_{slow}) + A_2*\exp(-t/\tau_{fast}) + I_{offset}$, where I_{ph} is the photo current, A_1 and A_2 are coefficients, t denotes the time, τ_{slow} and τ_{fast} are the slow and fast respective time constants, and I_{offset} is the current offset level. At 1 V bias, the contribution from the slow (τ_{slow}) and the fast component (τ_{fast}) and the respective values of A_1 and A_2 are comparable. However, at a higher bias voltage (Figure S4b), $A_2 << A_1$ indicates that the τ_{fast} component dominates, due to which the decay time declines rapidly. The rise time corresponds to the change in current from 0 to 100% and was calculated at 80 ms.

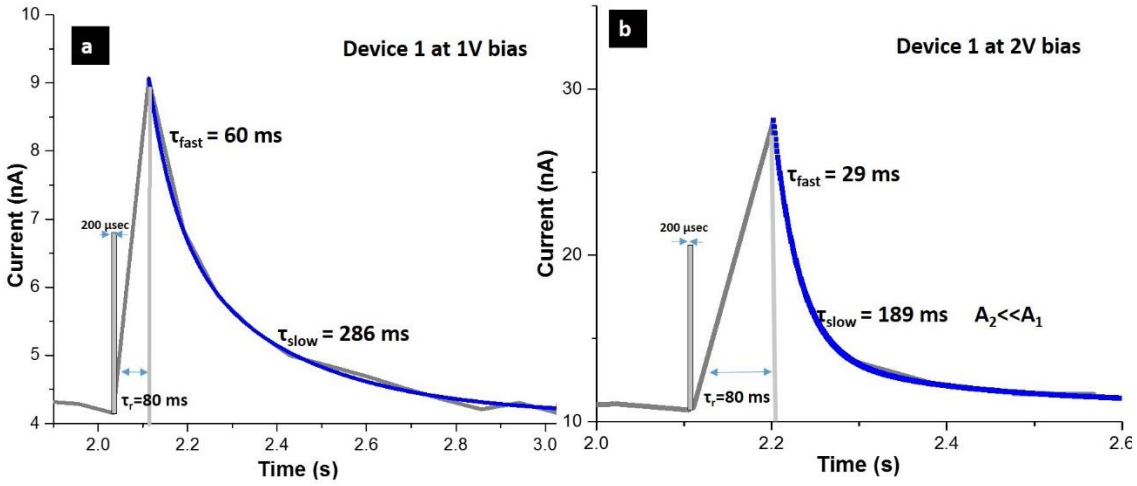

Figure S4. The calculation of the rise time and the decay time of Device 1 at the applied bias of (a) 1 V and (b) 2 V.

S4. Wavelength dependence of responsivity of the device

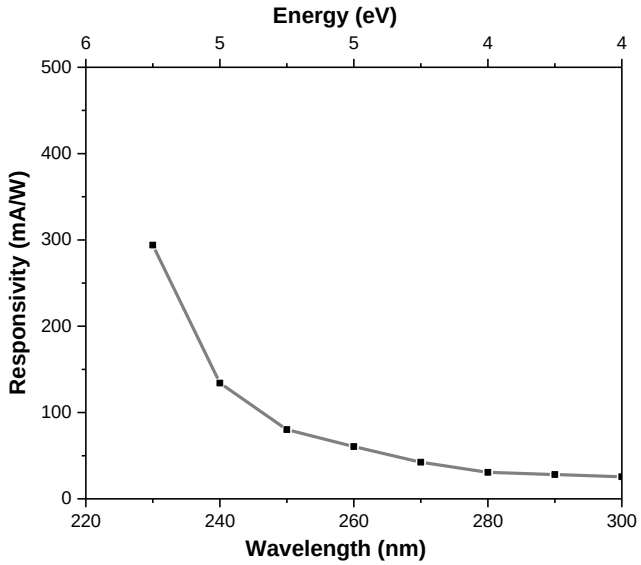

Figure S5. Shows the wavelength dependence of the responsivity.

We have performed wavelength dependence of the responsivity on Device 2. We have used Xenon lamp (AM 1.5G) and monochromator to perform the wavelength dependency. It can be noticed

that the responsivity of the Device 2 drastically falls above 260 nm illumination. This confirms the visible blindness of the device.

S5. Current-Voltage (IV) characteristics of the device 1

I−V characteristics of Device 1 are shown in Figure S6 under both dark and 224 nm illumination. The I−V results seem to indicate semi-Ohmic characteristics under illumination, possibly overcoming shallow Schottkey barrier with Ti electrodes.

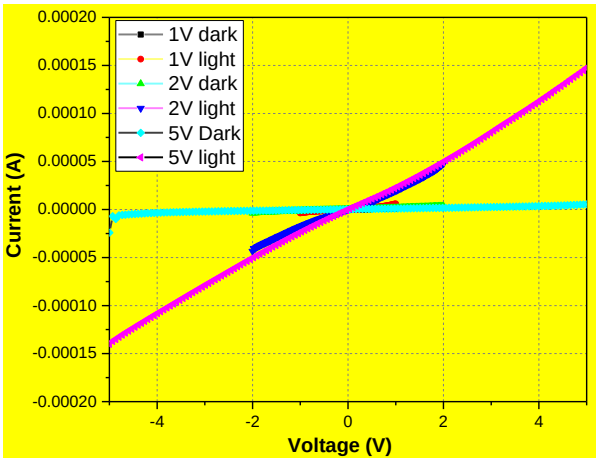

Figure S6. The I−V curve of Device 1 with and without CW 224 nm illumination was measured by Kiethley 2400 sourcemeter. 1000 W Xenon (Newport 66923) white light source was coupled with monochromator to produce 224 nm illumination, as our pulsed laser cannot be used for I−V measurements.

S6: Stability of the device over long DUV exposure time

The photocurrent generation was measured by the Kiethley 2400 apparatus. A 1000 W Xenon (Newport 66923) white light source was coupled with monochromator to produce 224 nm continuous illumination. The device was exposed to DUV illumination for almost half an hour and we could not see any significant changes over time, as shown in Figure S7. The change of the

photocurrent over time remains lower than 0.5%. This experiment was carried out in ambient conditions. The slight change in the photocurrent can be attributed to and the lamp's illumination stability.

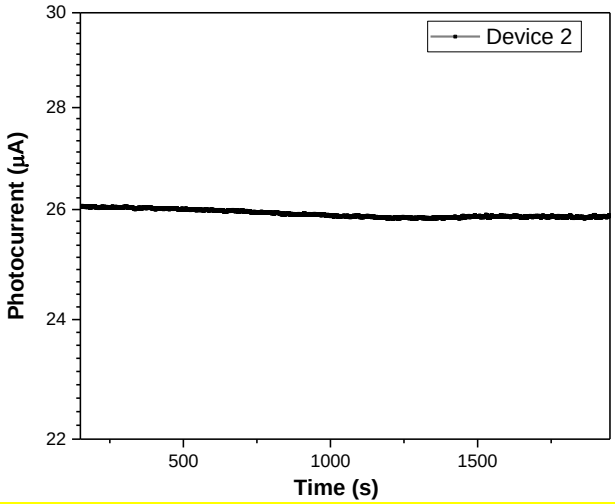

Figure S7. Photocurrent of the device 2 under 224 nm continuous illumination.

Reference

[1] Xiong G., Pal U., Serrano J., Ucer K., Williams R. Photoluminesence and FTIR study of ZnO nanoparticles: the impurity and defect perspective. *physica status solidi (c)* 3 (2006), 3577-3581.

[2] Singh SC., Gopal R. Synthesis of colloidal zinc oxide nanoparticles by pulsed laser ablation in aqueous media. *Physica E: Low-dimensional Systems and Nanostructures* 40 (2008), 724-730.

[3] Martinez CR, Vick JR, Perales O, Singh S. Cytotoxic studies of PEG functionalized ZnO Nanoparticles on MCF-7 cancer cells, Cancer Nanotechnology, 3 (2011), 420-423.

[4] Liu X, Du H, Sun XW. High-performance photoresponse of carbon-doped ZnO/reduced graphene oxide hybrid nanocomposites under UV and visible illumination. *RSC Advances* 4(2014), 5136.

[5] Muthulingam S, Bae KB, Khan R, Lee I-H, Uthirakumar P. Improved daylight-induced photocatalytic performance and suppressed photocorrosion of N-doped ZnO decorated with carbon quantum dots. *RSC Adv* 5 (2015), 46247-46251.

[6] Mishra DK, Mohapatra J, Sharma MK, Chattarjee R, Singh SK, Varma S*, et al.* Carbon doped ZnO: Synthesis, characterization and interpretation. *Journal of Magnetism and Magnetic Materials* 329 (2013),146-152.

[7] Yoshikawa M, Inoue K, Nakagawa T, Ishida H, Hasuike N, Harima H. Characterization of ZnO nanoparticles by resonant Raman scattering and cathodoluminescence spectroscopies. *Applied Physics Letters* 92(2008), 113115.

[8] Nemade K, Waghuley S. UV–VIS spectroscopic study of one pot synthesized strontium oxide quantum dots. *Results in Physics* 3(2013),52-54.

[9] Guo F, Yang B, Yuan Y, Xiao Z, Dong Q, Bi Y. A nanocomposite ultraviolet photodetector based on interfacial trap-controlled charge injection. *Nature nanotechnology* 2012; 7(12): 798-802.

[10] Sharma A, Bhattacharyya B, Srivastava A, Senguttuvan T, Husale S. High performance broadband photodetector using fabricated nanowires of bismuth selenide. *Scientific reports* 6 (2016),19138.

[11] Dai W, Pan X, Chen C, Chen S, Chen W, Zhang H, et al. Enhanced UV detection performance using a Cu-doped ZnO nanorod array film. *RSC Advances* 2014; 4(60): 31969-31972.

[12] Zhou H, Li L, Chen H, Guo Z, Jiao S, Sun W. Realization of a fast-response flexible ultraviolet photodetector employing a metal–semiconductor–metal structure InGaZnO photodiode. *RSC Advances* 2015; 5(107): 87993-87997.

[13] Rauch, T., Spectral enhancement of organic photodetectors. KIT Scientific Publishing: 7 (2014),150-152.